International Conference on Nuclear Data for Science and Technology 2007
DOI: 10.1051/ndata:07327

Production of noble gas isotopes by proton-induced reactions on Mg, Al, Si, Fe, Ni, Pb, and Bi

I. Leya[1,a], K. Ammon[1], B. Lavielle[2], E. Gilabert[2], R. Wieler[3], J.-C. David[4], and R. Michel[5]

[1] Physikalisches Institut, University of Bern, Bern, Switzerland
[2] Universités Bordeaux 1 & 2 – UMR 5084 CNRS, Gradignan Cedex, France
[3] Institut for Isotope Geology, ETH Zürich, Zürich, Switzerland
[4] DSM, DAPNIA/SPhN, CEA Saclay, France
[5] Center for Radiation Protection and Radioecology, University Hannover, Germany

Abstract. We measured integral thin target cross sections for the proton-induced production of He-, Ne-, and Ar-isotopes from Fe and Ni and of He-, Ne-, Ar-, Kr-, and Xe-isotopes from Bi from the respective reaction thresholds up to 2.6 GeV. Iron and Ni are important structural materials for the planned ADS/EA systems and Bi is a major constituent for planned spallation neutron sources. In addition, we give new data for the production of ^{3}He from Mg, Al, Si, and Pb by revising earlier data and considering now ^{3}H diffusive losses and new information for the ^{3}H/^{3}He branching ratios. The data are compared to results from theoretical nuclear model codes.

1 Introduction

Integral thin target cross sections for the production of residual nuclides are one of the basic data for modelling the activation yields in mixed particle fields, whereas the basic applications range from astro-, cosmo-, and geochemistry over medicine to the field of accelerator technology. In addition, in recent years spallation neutron sources were built in various countries and accelerator based nuclear transmutation (ADS), e.g., [1,2], and energy amplification (EA), e.g., [2,3], devices were proposed. However, for the reliable modelling of production rates for residual nuclides the differential particle spectra and the excitation functions of the relevant nuclear reactions have to be known. While calculating differential particle spectra using state-of-the-art Monte Carlo codes is now very reliable, the thus calculated cross sections are accurate within a factor of 2 at best, which is not sufficient for most applications.

Here we present thin target cross sections for the proton-induced production of He-, Ne-, and Ar-isotopes from Fe and Ni and of He-, Ne-, Ar-, Kr-, and Xe-isotopes from Bi from the respective reaction thresholds up to 2.6 GeV. In addition, we give here new revised cross sections for the production of ^{3}He from Mg, Al, Si, and Pb. For these elements revisions of the data published earlier by us [4,5] are necessary because new information about ^{3}H diffusive losses during irradiation and/or storage of the samples [6] and new ^{3}H/^{3}He branching ratios [6,7] showed up. The new experimental results are also compared to theoretical excitation functions calculated by INCL4/ABLA [8,9].

2 Experimental

Target material: High-purity materials were used as targets to avoid interfering reactions from impurities. Each target was carefully cleaned and weighted before irradiation and noble gas measurement. The targets were supplied by Goodfellow, UK.

Irradiations: The data presented here are obtained in 30 irradiation experiments performed between 1991 and 1997. The irradiations took place at the SATURNE synchrocyclotron of the Laboratoire National Saturne at Saclay, France (LNS, $E > 200$ MeV), The Svedberg Labo-ratory at Uppsala, Sweden (TSL, 70 MeV $< E <$ 200 MeV), and the Paul Scherrer Institute at Villingen, Switzerland (PSI, $E <$ 72 MeV). For proton energies below 200 MeV the stacked-foil technique was used, since the influences of secondary particles on the production of the nuclides studied here can be neglected. For the irradiation experiments above 200 MeV we used the mini-stack approach to reduce secondary particle effects. The flux densities were either determined via the reaction ^{27}Al(p,3p3n)^{22}Na using cross sections given by [10,11] or via the reaction ^{65}Cu(p,n)^{65}Zn [12]. In cases where the fluxes could be determined via ^{22}Na and ^{65}Zn the agreement was within the experimental uncertainties, e.g., within 5–7%.

Noble gas measurements: The noble gas isotopic concentrations were measured by static noble gas mass spectrometry. After being loaded into the extraction system the samples were preheated under vacuum in order to release atmospheric surface contamination. The Mg, Al, Si, Pb, and Bi samples were measured at the ETH Zürich. The Fe and Ni samples were measured at the Universities of Bern and Bordeaux. The gases were released by heating the samples to temperatures slightly above the melting temperature. To clean the gases Zr-Ti, Al-Ti and/or Ti getters were used. He-Ne, Ar, and Kr-Xe fractions were separated using cryogenic traps and measured separately [4,13]. The total uncertainties include the uncertainties of the mass and the thickness of the target foil, the uncertainties of the noble gas concentrations (blank corrections, calibrations), and the uncertainties of the monitor cross sections.

[a] Presenting author, e-mail: ingo.leya@space.unibe.ch

Table 1. Cross sections for the proton-induced production of ^{3}He from Mg and Al.

Energy [MeV]	Sigma [mb]	Energy [MeV]	Sigma [mb]
from magnesium		180 ± 1	11.7 ± 0.6
14.7 ± 0.8	0.06 ± 0.01	307 ± 1	19.6 ± 1.1
19.8 ± 0.8	0.36 ± 0.03	380 ± 1	22.0 ± 1.8
24.7 ± 0.7	2.45 ± 0.14	1600 ± 1	47.9 ± 3.9
31.7 ± 0.7	6.41 ± 0.37	*from aluminum*	
33.8 ± 0.6	7.13 ± 0.68	41.5 ± 0.4	7.96 ± 0.48
34.5 ± 0.7	7.17 ± 0.40	109 ± 1	11.9 ± 0.8
41.2 ± 0.6	7.73 ± 0.45	120 ± 1	13.1 ± 0.8
50.0 ± 0.8	10.4 ± 0.6	137 ± 1	14.2 ± 0.9
70.3 ± 0.5	12.0 ± 0.6	179 ± 1	13.3 ± 0.9
116 ± 1	15.4 ± 0.9	299 ± 1	18.4 ± 1.1
137 ± 1	14.6 ± 0.8	397 ± 1	21.9 ± 1.3

Table 2. Cross sections for the proton-induced production of ^{3}He from Si and Pb.

Energy [MeV]	Sigma [mb]	Energy [MeV]	Sigma [mb]
from silicon		95.5 ± 1.5	4.71 ± 0.77
31.3 ± 1.1	5.29 ± 0.31	105 ± 2	5.07 ± 0.82
80.7 ± 1.6	17.1 ± 1.0	114 ± 2	5.65 ± 0.90
98.8 ± 1.4	17.8 ± 1.0	122 ± 2	5.03 ± 0.82
112 ± 1	16.2 ± 0.9	130 ± 1	5.44 ± 0.88
123 ± 1	16.2 ± 0.9	144 ± 1	6.48 ± 1.05
136 ± 1	18.9 ± 1.1	158 ± 1	5.82 ± 0.94
179 ± 1	17.8 ± 1.1	171 ± 1	6.76 ± 1.04
317 ± 1	22.8 ± 1.5	240 ± 2	10.3 ± 1.8
317 ± 1	22.5 ± 1.4	273 ± 1	9.71 ± 1.14
388 ± 1	28.3 ± 1.4	322 ± 2	12.6 ± 1.7
1600 ± 1	71.1 ± 3.9	554 ± 2	20.6 ± 2.8
from lead		759 ± 2	31.5 ± 4.6
44.2 ± 0.9	2.78 ± 0.33	993 ± 1	31.7 ± 4.0
57.2 ± 0.8	4.12 ± 0.48	1163 ± 1	51.1 ± 7.5
65.5 ± 0.7	-	1395 ± 1	70.1 ± 8.7
76.5 ± 1.8	4.00 ± 0.62	1567 ± 1	63.8 ± 8.9
87.0 ± 1.8	4.46 ± 0.72	2595 ± 1	97.6 ± 12.5

3 Results

The revised cross sections for the proton-induced production of ^{3}He from Mg, Al, Si, and Pb are given in tables 1 and 2. Note that the cross sections given here replace our earlier data [4,5], which were not corrected for diffusive losses and/or based on incorrect ^{3}H/^{3}He branching ratios. The cross sections for the target elements Mg, Al, and Si are calculated assuming that diffusive losses follow a simple exponential law with the constant D. For the dimensionless ratio D/λ we use 2.6, 0.16, and 0.014 for Mg, Al, and Si, respectively [6]. Thereby λ is the decay constant of ^{3}H.

For the ^{3}H/^{3}He branching ratios we use 1.20, 1.28, 1.16, 7.18, and 7.18 for Mg, Al, Si, Pb, and Bi, respectively [6,7].

The cross sections for the production of ^{3}He from Pb and Bi are not corrected for ^{3}H diffusive losses, since currently no information for the D/λ-ratios are available. All ^{3}He cross sections given here are for the direct production of ^{3}He, i.e., without any contributions from the radioactive isobar ^{3}H.

Table 3. Cross sections for the proton-induced production of ^{3}He and ^{4}He from Bi.

	Cross section [mb]	
Energy [MeV]	^{3}He	^{4}He
102 ± 2	6.25 ± 0.94	109 ± 8
129 ± 2	7.31 ± 1.03	135 ± 12
134 ± 2	7.61 ± 1.04	168 ± 12
155 ± 2	5.56 ± 0.77	112 ± 8
161 ± 1	8.01 ± 1.05	162 ± 12
236 ± 2	8.88 ± 1.64	-
278 ± 1	6.65 ± 0.91	173 ± 12
319 ± 2	8.34 ± 1.71	225 ± 37
758 ± 2	26.9 ± 4.4	220 ± 36
999 ± 1	31.6 ± 3.9	813 ± 59
1161 ± 2	36.0 ± 5.9	857 ± 68
1398 ± 1	74.1 ± 9.9	1609 ± 114
1565 ± 2	47.8 ± 7.0	1231 ± 87
2589 ± 1	91.6 ± 12.4	2029 ± 161

The database for Bi is fairly complete by now. However, here we give as tables only cross sections for the production of ^{3}He and ^{4}He, because those data are most badly needed for the design of ADS/EA systems. All other data are given in figures only. For Fe and Ni some of the cross sections are still preliminary and we decided to give all data in figures only. However, two papers giving all data and detailed discussions are currently prepared.

Helium: The cross sections for the proton-induced production of total He from Mg, Si, Fe, Pb, and Bi measured by our collaboration are shown in figure 1. In general, the data agree well with results from other authors. We therefore focus on some systematic aspects without extensive comparisons with earlier data. The excitation functions get steeper with increasing target mass. For example, the cross sections for the production of He from Mg increase by only a factor of 2 when increasing the proton energy from 50 MeV to 1.6 GeV. In contrast, the data for Pb increases by two orders of magnitude in the same energy range. Higher cross sections at lower energies for lighter target elements can easily be explained considering the Coulomb-barriers. As an example, to overcome the Coulomb-barrier of Mg a ^{4}He particle must have more than 4.5 MeV; for Pb the energy increases to more than 21 MeV, therefore significantly preventing ^{4}He emission at low excitation energies. In addition, neutron emission and fission, which are competing reaction channels to ^{4}He emission, are important for heavy target elements, further reducing their He cross sections at low excitation energies. Higher cross sections for heavy elements are easily explained by their higher reaction cross sections. For example, the reaction cross section for Bi is about 4.5 times higher than for Mg. However, there is one notable exception to the discussed systematic. The cross sections for He production from Bi at energies below 200 MeV are significantly, i.e., by about a factor of 2, higher than the data for Pb. While smaller differences are expected due to slightly different reaction cross sections and Coulomb-barriers (see above), differences by about a factor of 2 found

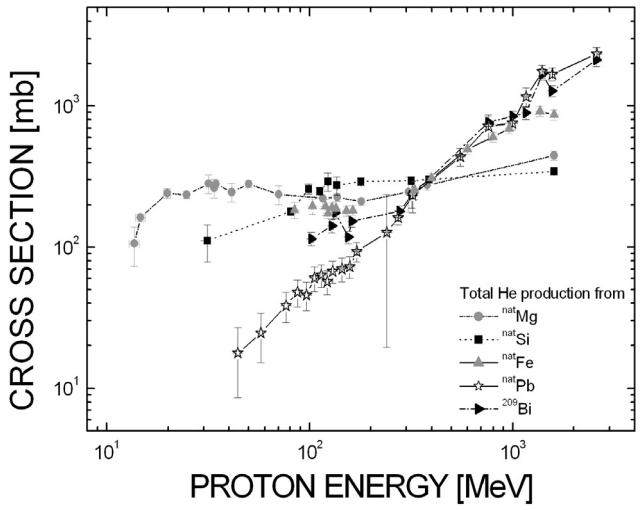

Fig. 1. Cross sections for the proton-induced production of total He from Mg, Si, Fe, Pb, and Bi.

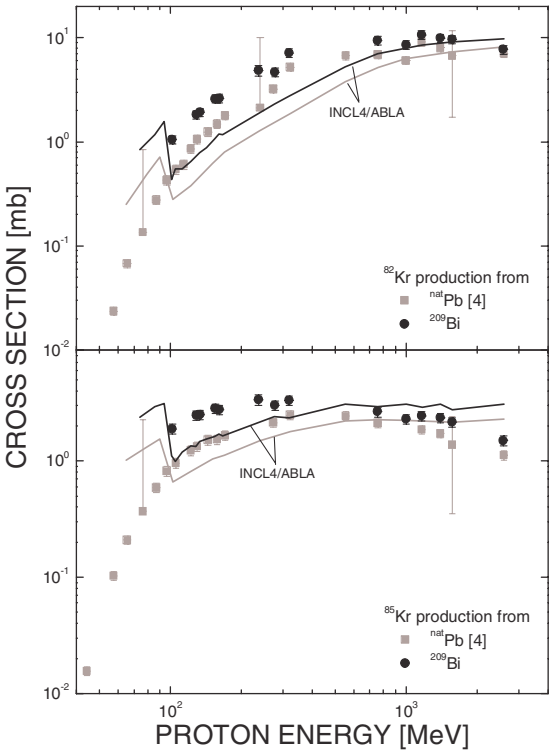

Fig. 2. Excitation functions for the proton-induced production of ^{82}Kr (upper panel) and ^{85}Kr (lower panel) from ^{nat}Pb (ref. [4], grey symbols) and ^{209}Bi (black symbols), respectively. The results of INCL4/ABLA calculations are shown as straight lines.

by us are not easy to understand. However, we can exclude that the obvious too high Bi data are due to experimental artefacts, as blank contributions are only very minor and the data have been obtained in three different runs, i.e., with three different spectrometer settings. We also checked whether recoil effects, which might be of importance because the 6 Bi targets were directly neighboured to Al catcher foils (unfortunately no other targets were available to us), are the reason for the too high He data. However, the expected recoil effects are much too small to explain the data. In addition, the high He cross sections for Bi are confirmed by results from an earlier study [14], which gives a ^{4}He cross section at 90 MeV in agreement with our data. We therefore have to face the fact that the production of He from Bi below 200 MeV might be up to 2 times higher than from Pb. At higher energies the cross sections for both target elements are, as expected, very similar.

Neon and Argon: For Pb and Bi the ^{21}Ne excitation functions above ~300 MeV are very similar, both showing a strong increase with projectile energy (not shown). Also similar for both elements, cross sections for the production of ^{21}Ne could be determined for energies down to ~100 MeV [4], where values of up to 0.1 mb are reached. However, in contrast to the Pb data, which were interpreted with respect to a possible lowering of the effective Coulomb-barrier [4], the interpretation of the Bi data is not straightforward, as recoil effects from neighboured Al foils cannot be excluded. For ^{36,38}Ar the cross section database for Pb and Bi is still very scarce. However, from the existing data we can conclude that the cross sections for both elements are very similar. Thanks to our new data the cross section database for Fe and Ni is fairly complete by now, which enable for a first time detailed studies of cosmogenic production rates in iron meteorites.

Krypton: Figure 2 exemplarily compares the excitation functions for the production of ^{82}Kr (upper panel) and ^{85}Kr (lower panel) from Bi (dark symbols) and Pb (grey symbols), respectively. The data for Pb are from [4]. Results from INCL4/ABLA calculations are shown as straight lines. As already discussed [4, 13] Kr isotopes are dominantly produced by hot or cold symmetric fission. Hot symmetric fission occurs early in the reaction process while the excited nucleus is still hot, i.e., at times early in the evaporation phase. We attribute the production of n-rich isotopes, e.g., ^{85}Kr, to hot symmetric fission. The n-poor isotopes, e.g., ^{82}Kr, are produced via cold symmetric fission, i.e., fission after the nucleus has almost completely de-excited at times later in the evaporation phase. The data for both symmetric fission channels clearly indicate that the cross sections for Bi are higher than for Pb, whereas the differences are higher at lower projectile energies.

At lower energies, i.e., below ~300 MeV, the cross sections from Bi are higher than from Pb by about a factor of 2. For energies above ~300 MeV the Bi data are only higher by about 20–40%. This is due to higher fission cross sections for Bi compared to Pb. For example, according to the systematic given by Prokofiev [15] the fission cross sections for Bi are higher than for Pb by about a factor of 2, 40%, and 30% at 100 MeV, 500 MeV, and 1.6 GeV, respectively. To summarize, the cross section database for Kr isotopes can consistently be explained assuming hot and cold symmetric fission as the dominant (only?) reaction mechanism and fission cross sections, which are (energy-dependent) higher for Bi compared to Pb.

Xenon: In figure 3 we exemplarily compare the excitation functions for the production of ^{126}Xe (upper panel) and ^{130}Xe (lower panel) from Bi (dark symbols) and Pb (grey symbols, [4]), respectively.

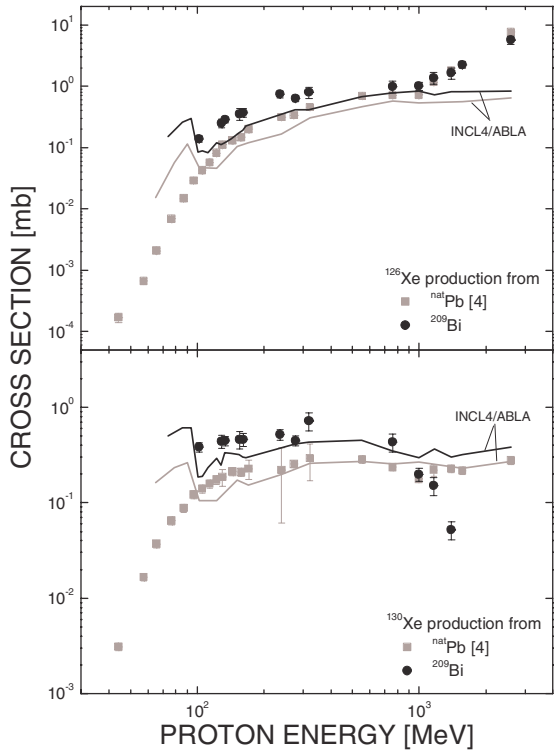

Fig. 3. Excitation functions for the proton-induced production of ^{126}Xe (upper panel) and ^{130}Xe (lower panel) from ^{nat}Pb (ref. [4], grey symbols) and ^{209}Bi (black symbols), respectively. The results of INCL4/ABLA calculations are shown as straight lines.

For the production of Xe isotopes from Pb and Bi two types of excitation functions can be distinguished. For some Xe isotopes, e.g., ^{130}Xe, asymmetric fission is the dominant (only?) reaction mechanism in the energy range studied here. However, at higher projectile energies, i.e., above 600-1000 MeV, some Xe isotopes, e.g., ^{126}Xe, can also undergo evaporation. By comparing the data for Pb and Bi one can see that the cross sections for evaporation are, as expected, very similar for both target elements (see upper panel in fig. 3). Considering the asymmetric fission mode the cross sections are higher for Bi compared to Pb, whereas the differences are higher at lower projectile energies. For example, the cross sections for the production of ^{130}Xe from Bi are higher than from Pb by factors 3.3, 1.8, and 1.4 at 100 MeV, 320 MeV, and 758 MeV, respectively. Similar to the discussion for Kr isotopes, some of the differences can be explained by the (energy-dependent) higher fission cross sections for Bi compared to Pb [15]. However, the differences in fission cross sections are not sufficient to explain all observed systematics. For example, the fission cross sections for Bi and Pb at 100 MeV differ by only a factor of 2, whereas the cross sections for ^{126}Xe measured here differ by more than a factor of 3. Furthermore, the data measured for ^{130}Xe, which is dominantly produced by asymmetric fission, cannot be explained at all. As shown in the lower panel of figure 3, the cross sections for ^{130}Xe from Bi are higher than from Pb up to energies of about 1 GeV. At higher energies there is a steep drop in the excitation function, making the cross sections at 1.4 GeV for Bi lower than for Pb by more than one order of magnitude. At the moment we have no explanation for the observed trend but the data indicate that the asymmetric fission mode does not only scale with the fission cross section. Further studies to better understand this systematic are needed.

4 Comparison with model calculations

The INC4/ABLA model describes most of the experimental data reasonable well, i.e., within a factor of 2. Notable exceptions are the production of ^{21,22}Ne and ^{36,38}Ar from Pb and Bi and the Xe isotopes above 1 GeV. The latter is due to the fact that we are close to the reaction threshold, i.e., close to the limit of applicability of INCL4/ABLA. Therefore, the comparison of measured and modelled data clearly indicate that experimental data are still needed because the predictive poser of nuclear model codes, though permanently improving, does still not allow to reliably predict the cross sections needed for most applications.

References

1. C.D. Bowman et al., Nucl. Instrum. Meth. A **320**, 336 (1992).
2. F. Carminanti et al., European Organisation for Nuclear research, CERN/AT/93-47(ET) 1993.
3. C. Rubbia et al., European Organisation for Nuclear Research, CERN/AT/95-44(ET) 1995.
4. I. Leya, R. Wieler, J.-C. David, S. Leray, L. Donadille, J. Cugnon, R. Michel, Nucl. Instrum. Meth. B **229**, 1 (2005).
5. I. Leya, H. Busemann, H. Baur, R. Wieler, M. Gloris, S. Neumann, R. Michel, F. Sudrock, U. Herpers, Nucl. Instrum. Meth. B **145**, 449 (1998).
6. I. Leya, F. Begemann, H.W. Weber, R. Wieler, R. Michel, Meteoritics and Planet. Sci. **39**, 367 (2004).
7. C.-M. Herbach et al., Nucl. Phys. A **765**, 426 (2006).
8. A. Boudard, J. Cugnon, S. Leray, C. Volant, Phys. Rev. C **66**, 044615 (2002).
9. A.R. Junghans, M. de Jong, H.-G. Clerc, A.V. Ignatyuk, G.A. Kudyaev, K.-H. Schmidt, Nucl. Phys. A **626**, 635 (1998).
10. J. Tobailem, D.H. de Lassus St. Genies, Note No. CEA-N-1466(5), Saclay, 1981.
11. G.F. Steyn, S.J. Mills, F.M. Nortier, B.R. Simpson, B.R. Meyer, Int. J. Radiat. Appl. Instrum. A **41**, 315 (1990).
12. R. Michel et al., Nucl. Instrum. Meth. A **129**, 153 (1997).
13. I. Leya, R. Wieler, J.-C. David, S. Leray, L. Donadille, J. Cugnon, R. Michel, Nucl. Instrum. Meth Phys. A **562**, 760 (2006).
14. J.R. Wu, C.C. Chang, H.D. Holmgren, Phys. Rev. C **19**, 698 (1979).
15. A.V. Prokofiev, Nucl. Instrum. Meth. Phys. Res. A **463**, 557 (2001).